ACS Photonics

Open Access

pubs.acs.org/journal/apchd5

Article

Dielectric High-Q Metasurfaces for Surface-Enhanced Deep-UV Absorption and Chiral Photonics

Shang Jie Shen,[#] Bo-Ray Lee,[#] Yu Chieh Peng, Yu Jie Wang, Yao-Wei Huang, Yuri Kivshar, and Ming Lun Tseng*

Cite This: *ACS Photonics* 2025, 12, 2955−2964

Read Online

ACCESS | Metrics & More | Article Recommendations | Supporting Information

ABSTRACT: Deep ultraviolet (DUV) light is critical for novel developments in molecular spectroscopy, clinical imaging, and nanolithography. It is promising to advance these technologies by leveraging dielectric metasurfaces' strong light manipulation capability. Realizing metasurfaces with high-quality-factor (high-Q) resonance in the DUV will be beneficial to those applications as they provide strong field enhancement and light confinement. However, due to the lack of high-index and low loss materials in this regime, it is considerably challenging to realize novel high-Q metasurfaces for sensing and light manipulation. We propose two device schemes wherein metasurfaces are strategically placed atop dielectric pillars or freestanding membranes. These configurations overcome the limitations associated with the low index contrast between the metasurfaces and substrates, thereby enabling the realization of high-Q resonance. We present multiple high-Q metasurfaces showcasing diverse DUV functionalities. The first application is spectrometerless biomolecular sensing. It is achieved through an array of high-Q metasurfaces exhibiting resonance associated with a quasi-bound state in the continuum (quasi-BIC). The strong field enhancement of the metasurfaces empowers the surface-enhanced deep-ultraviolet absorption (SEDUVA) of the biomolecules, thus allowing the detection of nanometer-thick analytes. Additionally, we introduce a nonlocal high-Q metasurface designed for DUV chiral photonics. It shows a narrow and near-unity peak in its DUV circular dichroism (CD) spectrum. These results establish a robust platform for developing novel nanophotonic devices and systems in the critical DUV wavelength range.

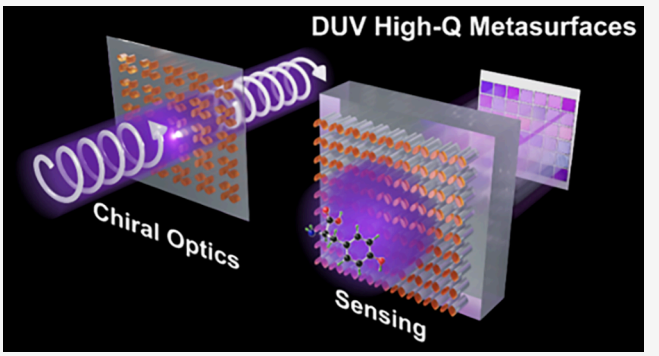

KEYWORDS: *metasurface, quasi-bound state in the continuum, nonlocal metasurface, deep ultraviolet light, chiral photonics, biosensing, surface-enhanced DUV absorption*

INTRODUCTION

Metasurfaces,[1−3] comprised of subwavelength resonance units known as meta-atoms, are a novel kind of versatile photonic device carefully designed to realize specific optical functionalities. Their applications cover a broad range, including light generation,[4−6] wavefront control,[7−13] photochemistry,[14,15] and biological/chemical sensing[2,16−18] across the ultraviolet to infrared spectral ranges. Recent focus has intensified on developing metasurfaces for deep ultraviolet light (DUV) applications, covering wavelengths from 200 to 300 nm. The high photon energy in this range (from 6.2 to 4.1 eV) holds promise for innovative biomolecular spectroscopy,[19−21] clinical imaging,[22,23] and advanced lithography.[24−26] For example, critical biomolecules, such as DNA, RNA, nucleotide bases, aromatic amino acids, and many drugs, show distinctive and strong absorption features in the DUV range.[19] Unlike infrared (IR) absorption, which is associated with vibrational states, biomolecules[19,27] and nanomaterials[28] exhibit DUV absorption due to electronic excitations within their chemical bonds, resulting in strong absorption cross sections and distinct spectral features. This higher absorption facilitates more efficient analyte detection. Additionally, the DUV absorption features of these molecules enable applications such as refractive index sensing,[29] *in vivo* molecular mapping,[30] and label-free cellular imaging.[22,30]

Previously, DUV metasurfaces and nanophotonic devices are typically made of aluminum, and their resonances are associated with localized surface plasmon resonances.[31] Due to the loss of the constituent material, DUV aluminum metasurfaces usually meet critical challenges such as low resonance quality and light-induced damage/photocorrosion.[32] One striking approach to this issue is replacing aluminum with low-loss dielectric materials. Many works have reported the

Received: October 10, 2024
Revised: March 22, 2025
Accepted: March 24, 2025
Published: April 1, 2025

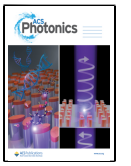

advantages of dielectric metasurfaces in the visible and infrared range, including low optical loss/heating, large laser damage threshold, and rich multipolar resonances. Using low-loss dielectric materials further allows for realizing high-quality factor (high-Q) resonances in the resulting metasurfaces. Such high-Q metasurfaces have advanced techniques in the visible and infrared regimes, including surface-enhanced infrared absorption spectroscopy (SEIRA),[33] solid-state high harmonic generation,[34] nanolasers,[35] and augmented reality devices.[36] Recent works have also shown the exciting possibility of using high-Q metasurface chiral optics, including control of circularly polarized state and the emission properties. While some works have explored ultraviolet wave control[26,37] and harmonic generation[4,11,38] through dielectric metasurfaces, realizing high-Q metasurfaces in this wavelength range remains challenging. This issue may result from the limited availability of high-index materials within the DUV spectrum. Only a handful of generally available dielectric materials, such as aluminum nitride (AlN) and hafnium oxide (HfO_2), exhibit suitable refractive indices ($n > 2$) and low optical losses ($k \sim 0$) for dielectric metasurfaces in the DUV range.[2] Still, the refractive index of these may not be sufficient for high-Q metasurface design in the DUV. The relatively low index of the constituent material contributes to low dielectric contrast between the resonant units and the substrate, which imposes a challenge for effectively achieving high-Q modes in DUV metasurfaces and limiting the development of relevant applications such as biosensing and light manipulation.

Here, we explore versatile strategies to realize functional high-Q metasurfaces in the DUV range. In the beginning, we discuss the impact of the substrate on DUV metasurfaces' resonance. To address the issue, we begin by strategically positioning the resonance unit cells of the metasurface atop dielectric pillars. This configuration minimizes substrate-induced loss by allowing the resonance to occur away from the substrate, resulting in a metasurface exhibiting a high-Q resonance. Through careful tuning of the geometric parameters of the unit cells, we realize an array of metasurface pixels (metapixels), expanding the high-Q resonance wavelength coverage across a significant portion of the DUV range. The strong resonance field produced by the metapixels enhances the absorption features of the adjacent biolayer at specific DUV wavelengths, which is similar to, but yet demonstrated, the counterparts SEIRA[17,39,40] in the mid-infrared (mid-IR) range. General sensing spectroscopy typically relies on Raman scattering, photoluminescence, and absorption to detect and distinguish biomolecules. While metasurfaces have significantly enhanced the performance of the first two methods in the DUV,[20] their potential for DUV molecular absorption enhancement for sensing applications remains underexplored. Here, we demonstrate that with the assistance of reported metapixels, surface-enhanced DUV absorption (SEDUVA) enables the biosensing of deposited analytes with thicknesses of only a few nanometers. Subsequently, we demonstrate a second device scheme involving the placement of the metasurface on a freestanding membrane. This membrane provides a near-unity dielectric background for the metasurfaces atop, thereby enabling the high-Q resonances. To showcase, we report a nonlocal chiral metasurface that exhibits near-unity DUV circular dichroism with a Q factor close to 10000. Our proposed device schemes open a path for realizing novel high-Q metasurfaces for widespread use in DUV technologies and relevant applications.

RESULTS AND DISCUSSION

Dependence of the Substrate Index. We investigated the challenges of using common dielectric materials and substrates to realize high-Q metasurfaces in the DUV range. By using Ansys Lumerical FDTD, we simulated and analyzed the optical properties of the metasurfaces reported in this work. In the simulations, the incident light propagated along the z-axis and was x-polarized. To understand the substrate's impact, we varied its refractive index (n_s) from 1 to 1.285 in steps of 0.0189 and calculated the optical response of the high-Q metasurface atop. Figure 1a shows the unit cell design, which

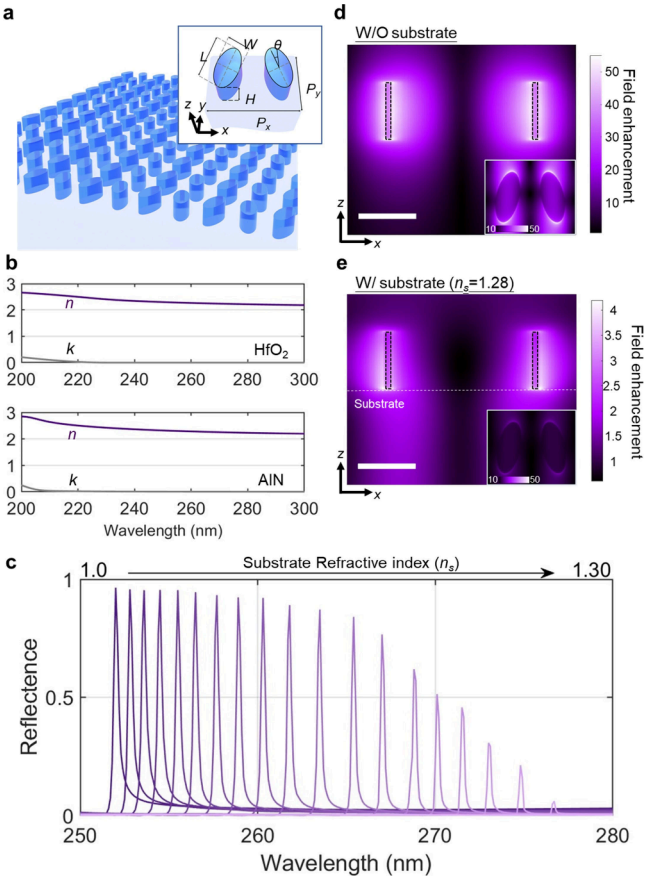

Figure 1. Impact of the substrate for DUV high-Q metasurface. (a) Schematic of the metasurface on an infinitely thick substrate. Inset: The unit cell. P_x = 212.6 nm, P_y = 151.4 nm, H = 60 nm, L = 102.6 nm, W = 51.3 nm, θ = 15°. (b) The optical constants of HfO_2 and AlN. (c) Reflectance spectra of the metasurface versus the refractive index of the substrate. (d) Enhanced electric field distribution of the unit cell in vacuum. (e) Enhanced electric field distribution of the unit cell on a substrate with a refractive index (n_s) 1.28. Note the range in the bottom panel was adjusted so the field profile can be clearly seen. The black dash lines in (d) and (e) indicate the boundaries of the HfO_2 particles. The white dashed line indicates the boundary between the substrate and the metasurface. Scale bar: 50 nm.

features elliptical nanoresonator pairs with a mutual rotation angle θ. This design breaks the in-plane symmetry, enabling the excitation of a high-Q resonance associated with the quasi-bound state in the continuum (quasi-BIC).[41−43] In this test, to exclude the effect of the dispersion of the constituent material on the metasurface's resonance properties, we set the refractive index as 2.1. In the simulations for other reported devices in this work, we used the optical constants of HfO_2 (the top panel

https://doi.org/10.1021/acsphotonics.4c01960
ACS Photonics 2025, 12, 2955−2964

in Figure 1b). We also confirm the feasibility of AlN (the bottom panel in Figure 1b) for the designs, see Supporting Information. Figure 1c shows that the resonance strength of the quasi-BIC mode deteriorates significantly as the substrate's refractive index increases, with peak reflectance dropping sharply, especially when the refractive index of the substrate is larger than 1.2 (see Figure S3a in Supporting Information). When n_s is larger than 1.28, the resonance feature is entirely quenched. To understand this impact, we simulated the field distribution within the meta-atom in vacuum and on a substrate (n_s = 1.28). As shown in the insets of Figure 1d,e, the meta-atoms show similar quadrupole patterns for both cases, which are optically dark and characteristic of the quasi-BIC resonance.[41] However, the field enhancement is much weaker with the substrate, with the maximum value decreasing from 50.5-fold to less than 5-fold. Figure 1d,e show the cross-sectional electric field distribution at the nanoellipse tips, without and with a substrate. Without a substrate, the resonant field is confined around the meta-atom surface. With a substrate, the field penetrates into it, indicating that the substrate may introduce an additional loss channel for the resonance. We can understand the impact of the substrate by considering the displacement current induced in a dielectric material. The displacement current in a dielectric material can be described as

$$I_D = \varepsilon \frac{\partial \Phi}{\partial t} \quad (1)$$

where I_D is the displacement current, ε is the dielectric constant of the material, and Φ is the electric flux in the material.[44] A large refractive index in the substrate will enable a significant optical response and coupling with the metasurface, creating a strong loss channel for optical energy and deteriorating resonance quality. The results in Figure 1 demonstrate that insufficient contrast between the constituent material and substrate impacts resonance quality, causing a critical issue in designing DUV high-Q nanophotonic devices. Notably, in the visible and IR regimes, several works also observed similar results in the deterioration of the high-Q resonances when the devices are placed on the substrates.[45−47] While this issue can be effectively mitigated in the other wavelength regimes by using constituent materials with larger indexes (*e.g.*, Si), it turns out to be much more challenging in the DUV regime, where high-index materials are not commonly available. General DUV photonic substrates like MgF_2 and CaF_2 have refractive indices[48,49] much higher than the maximum simulated value of 1.285 in the test, making high-Q metasurfaces using common DUV dielectric materials challenging to achieve. Solutions include reducing the coupling between the substrate and metasurface or minimizing the substrate's optical response.

Metasurfaces on Dielectric Pillars. The first reported method allowing the excitation of high-Q resonance in DUV metasurfaces involves positioning the unit cells on low-index dielectric pillars. Figure 2a shows a schematic illustration of the metasurface design. The unit cells made of HfO_2 are individually placed on SiO_2 pillars. Despite the proposed design's relatively high aspect ratio for the unit cell, fabrication is feasible using established processes for metalenses,[50,51] electronic devices,[52,53] and other optoelectronic applications.[54−56] The proposed on-pillar high-Q metasurfaces can be fabricated using lithography techniques to define etching masks, followed by dry etching. This process is similar to those

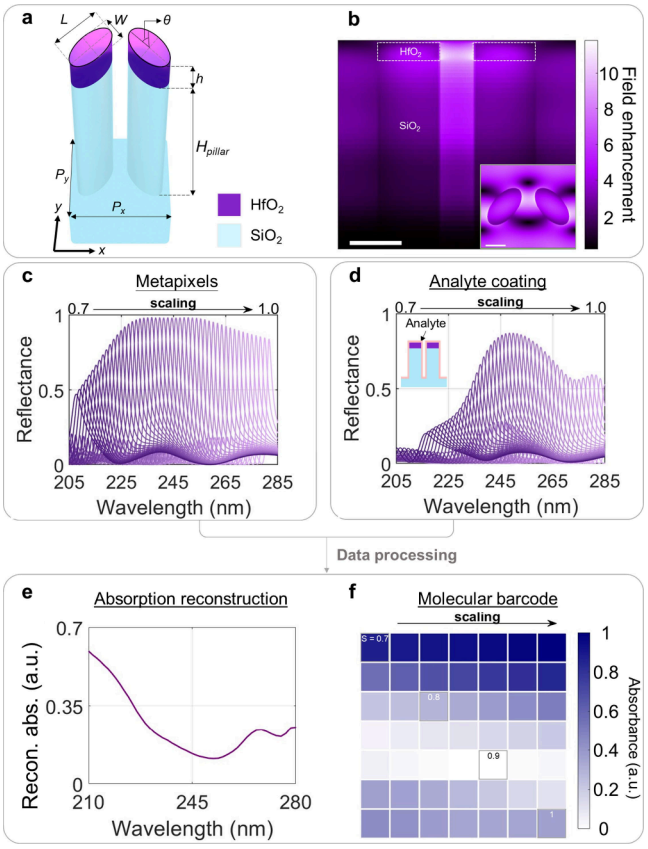

Figure 2. High-Q metapixels on dielectric pillars for SEDUVA. (a) Schematic and the geometric parameters of the unit cell. P_x = 235.4 nm, P_y = 256.8 nm, h = 60 nm, H_{pillar} = 700 nm, L = 128.4 nm, W = 64.2 nm, θ = 30°. (b) Enhanced electric field distribution of the meta-atom. Scale bar: 50 nm. (c) Reflectance spectra of the metapixels with different geometric scaling factors in steps of 0.0061. (d) Reflectance spectra of biolayer-coated metapixels. (e) Reconstructed absorbance (recon. abs.) spectrum of the tyrosine in the DUV range. (f) Molecular barcode corresponded to the DUV absorption of the tyrosine.

commonly employed in the fabrication of metalenses consisting of high-aspect-ratio dielectric pillars.[50,51] A detailed discussion is provided in Supporting Information. As can be seen in Figure 2b, the design enables strong field enhancement in the metasurface. The metasurface shows a field enhancement of more than 12.2-fold (*i.e.*, >100-fold in the intensity enhancement) at its resonance wavelength. The field is majorly confined around the meta-atoms and away from the substrate. The dielectric nanopillars prevent the metasurfaces' resonance field from penetrating the adjacent substrate, thus preventing the relevant optical loss.

To understand the influence of the pillar height to the metasurface's resonance, we changed the pillar's height and calculated the corresponding reflectance spectrum. It is found that, indeed, the peak reflectance and the quality factor attenuate when decreasing the height of the supporting pillars, see Figure S5 in Supporting Information. We observed that the SiO_2 pillars only provide a moderate effect on the resonance of the metasurface (see Figure S6 in Supporting Information). We further analyzed the properties of the metasurface when the sidewalls of the pillars are not perfectly vertical. In addition, for future experimental implementation, each metapixel must include a sufficient number of unit cells to maintain proper

https://doi.org/10.1021/acsphotonics.4c01960
ACS Photonics 2025, 12, 2955−2964

resonance properties and achieve an adequate signal-to-noise ratio in future experimental measurements, see Figure S30 in Supporting Information. We also verified that the metasurface shows adequate tolerance to this type of sample imperfection, see Figure S7 in Supporting Information.

The field enhancement generated from the metasurface is comparable to the previously reported plasmonic counterparts.[57,58] Such strong field enhancement is useful for biomolecular sensing in the DUV range. We demonstrate that the field enhancement and high-Q resonance properties of the reported metasurfaces can significantly enhance the absorption spectral features of biomolecules, enabling biomolecular sensing via SEDUVA. The working mechanism can be understood by using the absorption formula:

$$A_{\text{abs}} = \text{Im}[\varepsilon(\omega)]|E|^2 \tag{2}$$

where A_{abs} represents absorbed energy, $\text{Im}[\varepsilon(\omega)]$ is the imaginary part of the frequency-dependent dielectric function of the analyte, and E is the electric field surrounding the analyte. The strong light-matter interactions between the incident DUV light and biomolecules due to the electronic transitions (*e.g.*, n, π, or σ to π^* or σ^* molecule orbital transitions)[19] results in significant and distinctive DUV absorption features (larger $\text{Im}[\varepsilon(\omega)]$). When combined with the strong electric field enhancement (large $|E|^2$) provided by high-Q metasurfaces, the DUV absorption signals of biomolecules are effectively amplified, enabling sensitive detection of nanoscale biolayers. To demonstrate this, we designed 49 metasurface pixels (metapixels) whose planar geometric parameters are gradually scaled up, thus smoothly moving the resonance wavelength of the metapixels to cover the DUV absorption bands of biomolecules. In the simulation, a 5 nm-thick biomolecular layer is deposited on the metapixels. As shown in Figure 2c, the resonance wavelength of the metapixels smoothly shifts from 208 to 281 nm by scaling the unit cell size with a scaling factor ranging from 0.7 to 1. Here, we use biomolecule tyrosine as the target analyte. Tyrosine is a critical amino acid that plays an essential role in many bioprocesses. The optical constants of the tyrosine are from ref 27.

In the simulation, a 5 nm-thick tyrosine thin film was uniformly coated atop the metapixels, as depicted in the inset of Figure 2d. The spectra of the metapixels covered with the tyrosine film are shown in Figure 2d. The absorption of the tyrosine layer causes significant attenuation for specific spectra. The absorption features of the biolayer can be retrieved by analyzing the spectra. However, the metapixels' sensitivity may vary, which would cause issues in the spectrum analysis. To solve it, we simulated the reflectance spectra of the metapixels covered with a layer of model materials having different extinction coefficients. In the simulation (see Supporting Information), we fixed the refractive index of the material and calculated the reflectance spectra of the metapixels for $k = 0$ and 0.1, respectively. The ratio of the peak reflectance of each metapixel (defined as ξ_i, $i = 1, 2, 3, ..., 0.49$) from the two cases is subsequently calculated; see Figure S9 in Supporting Information. ξ_i are used to fix the sensitivity difference between the metapixels. Similar to the previous work[33,59] on surface-enhanced spectroscopy in the IR regime, by using the reflectance properties of the metapixels as the reference, the absorption information on the tyrosine detected by the metapixels can be analyzed by using

$$A_i = -\log\left(\frac{R_i'}{R_i \times \xi_i}\right) \tag{3}$$

where A_i is the retrieved absorbance of the tyrosine, R^i and R_i are the peak reflectance of the metapixel with and without the biolayer, respectively. The reconstructed absorbance spectrum of the tyrosine is shown in Figure 2e. The spectrum shows a good agreement with the extinction coefficient of the tyrosine, which corresponds to the absorption of the biolayer. This result confirms the capability of the reported method to enhance and reconstruct the spectral features associated with the analyte's DUV absorption. We further used the metapixels for sensing a 5 nm-thick DNA layer and successfully reconstructed the thin layer's absorption features (see Figure S10 in Supporting Information). We also demonstrate that the metapixels can detect ultrathin biomolecular layers and analyze their sensitivity, see Supporting Information. We note that, to demonstrate the sensing capability of the reported metapixels, we used biomolecules with well-characterized optical properties. However, the proposed sensing scheme can also assist in identifying and analyzing unknown analytes by comparing their spectra with previously reported molecular data, similar to the approaches used in SERS[60] and SEIRA[17,61] research. In practical sensing applications, techniques such as self-assembling,[39,62] and spin coating[63] can be used for preparing the analyte thin layers. Established methods for binding specific molecules to the surface of dielectric metapixels can be incorporated into experimental implementations to enhance selectivity.[64−67] For sensing processes involving multilayer captured molecules (*e.g.*, serial binding for antibodies and DNA) or molecule mixtures, analysis protocols[16,68,69] can be employed to distinguish the absorption features of individual molecules.

In principle, the metapixels can further enable spectrometer-less biosensing in the DUV range. By sending a broadband DUV light to the array coated with an absorptive biolayer, the individual metapixels show different resonance attenuation in their optical images. As the individual metapixels show a narrow resonance bandwidth, they serve as individual reporters which provide absorption information on the biolayer at specific wavelength windows. To confirm this, we converted the absorption value of the retrieved from the metapixels into different colors and plotted the result in Figure 2f. The image shows a specific barcode for the tyrosine film. This result confirms that by using the metapixels, the absorption property of biolayers can potentially be effectively detected and analyzed without DUV spectrometers. By integrating the metapixels with a DUV light source (*e.g.*, a DUV light-emitting diode), a DUV-compatible camera, and other relevant components, an imaging-based sensing device can be constructed, see Supporting Information for details. This imaging-based sensing approach may also find applications in mapping the molecular distribution in biological samples[23,30] or films. The proposed method offers unique advantages for many potential biology and material research applications as optical components for DUV spectrometers are generally pricy and limited in choice.

We reduced the height of the metapixels' SiO_2 pillars to 350 nm and performed biomolecular sensing tests, as shown in Figure S11 in Supporting Information. The results confirm that although the resonance strength is weaker with shorter supporting pillars, the metapixels still provide the capability for sensing nanometer-thick biomolecular layers. Adopting shorter pillars in the metapixel designs will significantly

https://doi.org/10.1021/acsphotonics.4c01960
ACS Photonics 2025, 12, 2955−2964

simplify the fabrication process and reduce costs, thereby enhancing the feasibility of future experimental implementations.

Metasurfaces on Freestanding Membranes. The second approach to realize DUV high-Q metasurfaces is to place the meta-atoms on a freestanding dielectric membrane. Freestanding dielectric membranes, fabricated using standard semiconductor processes,[70−72] have been widely utilized in biomedical analysis and electronic devices.[73−76] In nanophotonics, they work as the supporting layers for many metasurfaces created for biosensing,[70] optical signal switching,[77,78] nonlinear optics,[79] and light focusing.[70,80,81] Several previously reported methods have been employed to fabricate the on-membrane nanophotonic structures, each offering distinct advantages. For instance, a process combining electron beam or DUV lithography with double-side alignment and multiple dry etching steps is particularly effective for fabricating the reported metasurfaces.[70,80,82] This approach enables precise patterning and high structural fidelity. Additionally, focused ion beam (FIB) milling can be utilized to directly sculpt nanostructures on dielectric thin films deposited on commercially available freestanding membranes, providing an alternative fabrication route with high resolution and flexibility.[77] More details on the sample fabrication can be found in Supporting Information. Optically, freestanding membranes provide a near-unit effective index to the adjacent metasurface. This property is very beneficial for high-Q metasurface designs in the DUV range. We simulated the resonance properties of metapixels consisting of ellipse pairs on a freestanding SiO_2 membrane (Figure 3a). The metasurface

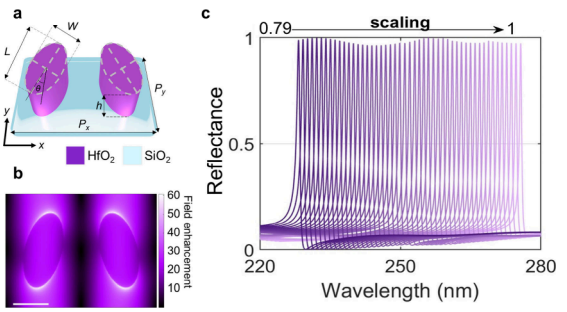

Figure 3. DUV high-Q metasurface on the freestanding membrane. (a) Schematic of the unit cell. P_x = 224.2 nm, P_y = 159.6 nm, h = 60 nm, L = 108.3 nm, W = 54.2 nm, θ = 15°. The thickness of the membrane: 15 nm. (b) The field enhancement simulation of the metasurface. The scaling factor is 0.947, and the resonance wavelength is ∼269.3 nm. Scale bar: 50 nm. (c) Reflectance spectra of the metasurface pixels (metapixels) on the membrane with different geometric scaling factors in steps of 0.0043.

shows a quasi-BIC mode with strong field enhancement (more than 30-fold) at 269.3 nm, as shown in Figure 3b. In addition, we also successfully shifted the resonance by imposing different scaling parameters on the unit cells. Similarly, by scaling the planar geometric parameters from 0.79 to 1, the high-Q resonance can be effectively tuned across the DUV range (Figure 3c). Due to the high transmittance, the membrane can be used as the observation window when there is a need to perform the optical measurement from the backside.[70] We simulated the reflectance spectra of the metasurfaces with incident light coming from the membrane side. The results confirm that the metasurfaces maintain high-Q resonances with backside excitation. These results are presented in Supporting Information. We also varied other geometric parameters, including the height of the unit cells and the membrane thickness, the lattice constants, and the particle size, to understand their influence on the resonance properties, see Supporting Information.

The metasurface-on-membrane configuration can enable on-demand optical functionalities in the DUV range. To showcase, we designed a metasurface showing a high-Q chiral BIC resonance. Chirality of matter pertains to the asymmetry or handedness exhibited by specific molecules or objects, distinguishing them as either left-handed or right-handed and influencing their interactions in various physical and chemical processes. Metasurfaces with chiral geometries exhibit strong circular dichroism (CD), characterized by distinct spectral responses under left- and right-circularly polarized (LCP/RCP) light excitations.[83−86] Maximizing the CD of a chiral metasurface in the DUV range holds significant potential for developing nanophotonic devices for novel light sources, sensing applications, and photochemistry. However, achieving planar metasurfaces with a strong CD response in the DUV range remains challenging; only a few examples have been demonstrated thus far, primarily in the infrared range.[87,88] Recent works have shown that enabling a strong chiral response is possible by introducing a nonlocal effect into the metasurface's resonance.[89,90] The flexibility of light control using the mutation interaction of the unit cells allows for designing a strong and narrowband chiral response in the metasurface. Figure 4a,b show the design of the metasurface.

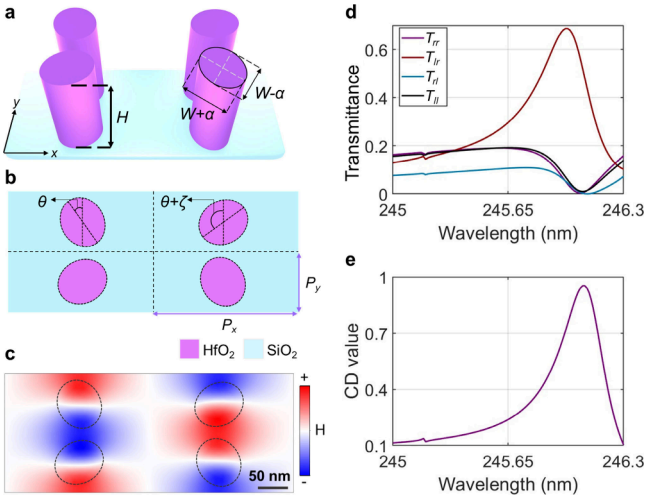

Figure 4. DUV chiral BIC Metasurface. (a) The side view and (b) the top view of four unit cells. W: 75.35 nm; α: 6.03 nm; H: 165.8 nm; P_x: 241.8 nm; P_y: 100.08 nm; θ: 67.5°; ζ: 90°. The unit cells on the left side are moved 6 nm leftward; meanwhile, the unit cells on the right side are moved 6 nm rightward. The thickness of the membrane is 13.5 nm. (c) The z-component magnetic field distribution of the unit cells. (d) Transmittance spectra of T_{ll}, T_{rr}, T_{rl}, and T_{lr}. (e) Corresponding CD spectrum of the metasurface.

Four resonance unit cells are assembled in a group. The metasurface's chiroptical properties can be effectively tuned by tuning its height, individual rotation angle, mutual displacement, and periodic constants. The multiple degrees of freedom in the designs combining the physics of bound state in the continuum allows for the realization of a metasurface showing an ultranarrow banded near-unity circular dichroism while

https://doi.org/10.1021/acsphotonics.4c01960
ACS Photonics 2025, 12, 2955−2964

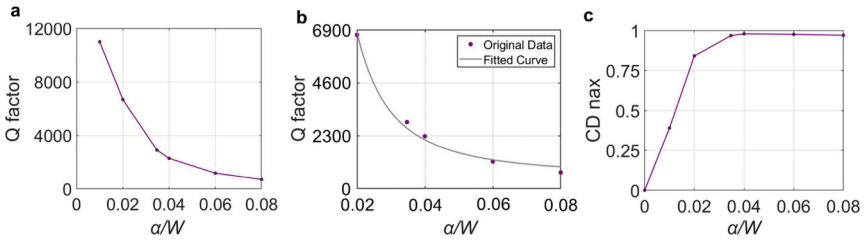

Figure 5. Effect of the in-plane asymmetry on the chiral BIC metasurface's properties. (a) The metasurface's quality factor versus the asymmetry parameter (α/W). (b) The fitted curve of the Q factor versus the asymmetry parameter (α/W). (c) The metasurface's maximum CD value versus the asymmetry parameter (α/W).

maintaining a high transmittance of the resulting metasurface. More design optimization analysis is shown in Supporting Information. Figure 4c shows the z-component magnetic field distribution around the unit cells at the resonance wavelength (245.9 nm) under RCP illumination from the bottom side. The metasurface shows a quadruple resonance at the resonance, which is optically dark for such an excitation configuration. Note that the reported design belongs to the type of nonlocal metasurface,[16,89] as the chiral BIC mode is enabled by the interactions between multiple meta-atoms in the array.

The nonlocal-resonance-induced chiroptical property of the reported metasurface can be observed in the spectral analysis. As shown in Figure 4d, under RCP illumination, the metasurface shows a sharp peak for the output component in LCP (the cross-polarized state) and a resonant dip for the component in RCP (the copolarized state). Meanwhile, with the LCP excitation, a dip for both the co- and cross-polarized components is observed. Notably, being different from intrinsic three-dimensional chirality, intrinsic planar chirality is always observed with circular conversion dichroism (CCD).[91−93] The result agrees with the previous observations and confirms the origin of the planar chirality of the reported metasurface. The selective excitation of the high-Q resonance results in a large CD of the metasurface. We calculated the circular dichroism of the metasurface by using the formula defined in ref 87:

$$\mathrm{CD} = \frac{(T_{rr} + T_{lr)} - ((T_{ll} + T_{rl)})}{(T_{rr} + T_{lr)} + ((T_{ll} + T_{rl)})} \tag{4}$$

where T_{ij} (i and j can be l or r, corresponding to LCP or RCP, respectively) is the transmittance with a polarization in the i state under the excitation in the j state. As shown in Figure 4e, the metasurface shows maximum circular dichroism close to 0.93 at 245.93 nm. It is the highest CD value from a nanophotonic device in the DUV range. The metasurface's property, which simultaneously exhibits high transmittance of specific light components and strong CD value, is beneficial for developing novel chiral devices. We further calculated the quality factor of the transmittance peak in the T_{lr} spectrum versus the asymmetry parameter, which is defined as the ratio between the unit cell's structural perturbation (α) and its width (W). The result shows that the high-Q resonance of the metasurface is highly sensitive to the structural symmetry (Figure 5a). The Q factor drops with an increasing asymmetry parameter, following the α^{-2} law (see the fitting curve, Figure 5b), which confirms that the observed high-Q resonance is associated with a quasi-BIC resonance.[41] The quality factor drops with the increased asymmetry parameter. In addition, the CD versus the asymmetry parameter is also calculated. As shown in Figure 5c, the result shows that the maximum CD value of the metasurface decreases when the asymmetry parameter is decreased, confirming the relation dependence of the metasurface's optical chirality on its mirror symmetry.

CONCLUSION

In response to the unmet need for high-quality-factor metasurfaces in the DUV range, we have developed two device schemes that effectively overcome the limitations of conventional designs, enabling novel functionalities and relevant applications in biosensing and chiral optics. The design schemes enable the high-Q resonances in metasurfaces made of moderate index materials and open up possibilities to realize novel nanophotonic devices. By using the reported design approaches, we show two on-demand optical functionalities that have not been investigated before in this high photon energy range. In principle, both reported device schemes are suitable for designing metasurfaces for SEDUVA and chiral optics, depending on application requirements, available fabrication tools, and device integration needs. SEDUVA offers several advantages and innovations. SEDUVA can be implemented using relatively low-cost DUV light-emitting diodes (LEDs), which are recently commercially available, for illumination. This approach would reduce the complexity of sensing systems and can open exciting possibilities for developing compact and novel devices for sensing, clinical diagnostics. The technique also has potential applications in material science, particularly for materials like polymers and 2D transition metal dichalcogenides,[28] which exhibit pronounced absorption peaks. The reported sensing scheme could be utilized for material quality inspection and investigation.

Compared with other DUV sensing techniques, a key practical advantage of SEDUVA is its simplified experimental setup, as it does not require optical filtering, enabling direct spectral readout through metapixel reflectance modulations. This feature, combined with the inherently larger absorption cross sections of molecules in the DUV range, enhances signal detection and analysis. Moreover, SEDUVA allows for image-based detection, offering a promising avenue for high-sensitivity, label-free molecular sensing. However, we would like to note that this method would not apply to novel materials with high energy bandgaps, as it primarily relies on the absorption properties of the analyte. The reported DUV high-Q metasurface presents exciting opportunities for exploring light-matter interactions across different coupling regimes, including the potential for strong coupling.[16] Its ability to confine light and enhance localized electromagnetic fields in the deep ultraviolet makes it a promising platform for studying molecular absorption dynamics and energy exchange.

https://doi.org/10.1021/acsphotonics.4c01960
ACS Photonics 2025, 12, 2955−2964

Future work could utilize these metasurfaces to probe the transition between weak and strong coupling regimes, uncovering new phenomena unique to the DUV spectral range.

Although both the on-pillar and on-membrane metasurfaces can be produced using fully CMOS-compatible processes, they have different instrumental requirements. Specifically, well-established processes for complementary metal-oxide-semiconductor (CMOS) imaging sensors (CIS) and memory devices can be adopted for the throughput of on-pillar metasurfaces, which require an etcher capable of producing pillar structures with straight, vertical sidewalls.[52] In contrast, large-scale fabrication of on-membrane metasurfaces requires a dry etching tool capable of performing deep reactive ion etching with the assistance of a double-sided alignment technique, drawing on knowledge from fabrication processes for microelectromechanical-systems (MEMS) based tunable nanophotonics[82] and metalenses.[70] From an application perspective, both device schemes show promise for developing miniaturized photonic systems with integrated devices. Metasurfaces on freestanding membranes can be integrated into microfluidic devices, with the transparent membrane serving as a window for backside observation. Additionally, incorporating MEMS techniques into the design allows for cascading multiple on-membrane metasurfaces with different functionalities into a single device and may also enable tunability of properties by applying external energy.[82] Meanwhile, on-pillar metasurfaces can be directly fabricated on top of photodetectors, such as CIS and single-photon avalanche diodes (SPADs), through additional film deposition, lithography, and etching. This offers exciting possibilities for realizing integrated nanophotonic devices and their applications, such as biosensing and light filtering. In addition, except for the applications investigated in the paper, the functionalities demonstrated by these metasurfaces hold great promise for many other DUV applications, including nonlinear optics, quantum optics, and photochemistry. Considering the utilization of industry-standard design schemes and materials in our device designs, we anticipate that large-scale fabrication of these metasurfaces can be efficiently accomplished using standard semiconductor processes.[70] This work opens up a new avenue for advancing the photonic technologies and the relevant applications in this critical wavelength range.

METHODS

Refractive Index Measurement. The refractive index and extinction coefficient of AlN and HfO_2 were measured by using a spectroscopic ellipsometers (M 2000, J. A. Woollam). The AlN thin film was deposited on a sapphire substrate by using PECVD. The HfO_2 film was deposited on a silicon substrate by using atomic layer deposition.

Numerical Simulations. The numerical simulations of the metasurface optical response were performed using commercial FDTD-based software Lumerical (Ansys). In the simulation, a periodic boundary condition was imposed along the x axis and y axis. For exciting the metasurfaces shown in Figures 1−3, the polarization is linear and along the x axis and incident from the top of the metasurfaces. For the chiral metasurface, the polarization is circular and incident from the membrane side. We used the ellipsometer data of AlN and HfO_2 in the simulation.

ASSOCIATED CONTENT

Data Availability Statement

The data that support the findings of this study are available from the corresponding author upon reasonable request.

Supporting Information

The Supporting Information is available free of charge at https://pubs.acs.org/doi/10.1021/acsphotonics.4c01960.

DUV high-Q metasurface using AlN; The impact of the substrate's property to the metasurface resonance; Fabrication process for the on-pillar metasurfaces; Dependence of the resonance on the pillar height; Simulation of the SiO_2 pillars; Tolerance to the tapered sidewalls of the pillars; Biosensing using the on-pillar metasurface pixels; Fabrication process for the on-membrane metasurfaces; Backside illumination of the on-membrane metasurfaces; Tolerance to the size deviation; Optimization of the chiral BIC metasurfaces designs; Surface-enhancement factor (SEF) calculation; Possible experimental setup for molecular barcode measurement; Discussion on the impact of the thin film nonuniformity; Noise considerations in reflection spectrum measurements; The effect of finite device size (PDF)

Optical constants of AlN (XLSX)

Optical constants of HfO_2 (XLSX)

AUTHOR INFORMATION

Corresponding Author

Ming Lun Tseng − *Institute of Electronics, National Yang Ming Chiao Tung University, Hsinchu 300093, Taiwan;* orcid.org/0000-0003-0418-8162; Email: mltseng@nycu.edu.tw

Authors

Shang Jie Shen − *Institute of Electronics, National Yang Ming Chiao Tung University, Hsinchu 300093, Taiwan*

Bo-Ray Lee − *Institute of Electronics, National Yang Ming Chiao Tung University, Hsinchu 300093, Taiwan*

Yu Chieh Peng − *Institute of Electronics, National Yang Ming Chiao Tung University, Hsinchu 300093, Taiwan*

Yu Jie Wang − *Institute of Electronics, National Yang Ming Chiao Tung University, Hsinchu 300093, Taiwan*

Yao-Wei Huang − *Department of Photonics, College of Electrical and Computer Engineering, National Yang Ming Chiao Tung University, Hsinchu 300093, Taiwan;* orcid.org/0000-0001-8983-413X

Yuri Kivshar − *Nonlinear Physics Centre, Australian National University, Canberra, ACT 2601, Australia;* orcid.org/0000-0002-3410-812X

Complete contact information is available at: https://pubs.acs.org/10.1021/acsphotonics.4c01960

Author Contributions

#These authors contributed equally to this work (S.J.S. and B.-R.L.). M.L.T. initiated the study. M.L.T., S.J.S., and B.-R.L. performed the simulations and analysis. Y.C.P. and Y.J.W. measured the optical constants of AlN. Y.-W.H. and Y.K. assisted with the data analysis and paper revision. M.L.T. supervised the project. M.L.T. and B.-R.L. wrote the paper.

Funding

National Science and Technology Council (NSTC 113-2636-M-A49-001, 113-2112-M-A49-025 113-2813-C-A49-134-M,

113-2221-E-260-007-MY3), Taiwan The Ministry of Education (Yushan Young Scholar Program), Taiwan Australian Research Council (Grant No. DP210101292), Australia International Technology Center Indo-Pacific (ITC IPAC), and Army Research Office (Contract FA520923C0023)

Notes

The authors declare no competing financial interest.

■ ACKNOWLEDGMENTS

The authors acknowledge support from the National Science and Technology Council (NSTC 113-2636-M-A49-001, 113-2112-M-A49-025, 113-2813-C-A49-134-M, 113-2221-E-260-007-MY3) in Taiwan, and the Center for Integrated Electronics-Optics Technologies and Systems, National Yang Ming Chiao Tung University. This work was also supported by the Higher Education Sprout Project of National Yang Ming Chiao Tung University and the Ministry of Education (MOE), Taiwan. M.L.T. and Y.-W.H. acknowledge the Yushan Young Scholar Program by the Ministry of Education (MOE), Taiwan, for the financial support. The authors are grateful to the support from the Center for Integrated Electronics-Optics Technologies and Systems, National Yang Ming Chiao Tung University and the Taiwan Semiconductor Research Institute (TSRI). The authors thank Mr. Ting Aa Hsu for his assist in preparing the HfO_2 film and the relevant refractive index measurement. Y.K. acknowledges support from the Australian Research Council (Grant No. DP210101292) and the International Technology Center Indo-Pacific (ITC IPAC) via Army Research Office (contract FA520923C0023).

■ REFERENCES

(1) Karawdeniya, B. I.; Damry, A. M.; Murugappan, K.; Manjunath, S.; Bandara, Y.; Jackson, C. J.; Tricoli, A.; Neshev, D. Surface Functionalization and Texturing of Optical Metasurfaces for Sensing Applications. *Chem. Rev.* **2022**, *122* (19), 14990−15030.
(2) Tseng, M. L.; Jahani, Y.; Leitis, A.; Altug, H. Dielectric metasurfaces enabling advanced optical biosensors. *ACS Photonics* **2021**, *8* (1), 47−60.
(3) Qiu, C. W.; Zhang, T.; Hu, G.; Kivshar, Y. Quo Vadis, Metasurfaces? *Nano Lett.* **2021**, *21* (13), 5461−5474.
(4) Semmlinger, M.; Zhang, M.; Tseng, M. L.; Huang, T. T.; Yang, J.; Tsai, D. P.; Nordlander, P.; Halas, N. J. Generating Third Harmonic Vacuum Ultraviolet Light with a TiO_2 Metasurface. *Nano Lett.* **2019**, *19* (12), 8972−8978.
(5) Kruk, S.; Kivshar, Y. Functional Meta-Optics and Nanophotonics Governed by Mie Resonances. *ACS Photonics* **2017**, *4* (11), 2638−2649.
(6) Suh, J. Y.; Kim, C. H.; Zhou, W.; Huntington, M. D.; Co, D. T.; Wasielewski, M. R.; Odom, T. W. Plasmonic bowtie nanolaser arrays. *Nano Lett.* **2012**, *12* (11), 5769−5774.
(7) Yu, N.; Capasso, F. Flat optics with designer metasurfaces. *Nat. Mater.* **2014**, *13* (2), 139−150.
(8) Tseng, M. L.; Hsiao, H. H.; Chu, C. H.; Chen, M. K.; Sun, G.; Liu, A. Q.; Tsai, D. P. Metalenses: Advances and Applications. *Adv. Opt. Mater.* **2018**, *6* (18), 1800554.
(9) Chang, C. M.; Tseng, M. L.; Cheng, B. H.; Chu, C. H.; Ho, Y. Z.; Huang, H. W.; Lan, Y.-C.; Huang, D.-W.; Liu, A. Q.; Tsai, D. P. Three-Dimensional Plasmonic Micro Projector for Light Manipulation. *Adv. Mater.* **2013**, *25* (8), 1118−1123.
(10) Hsiao, H.-H.; Chu, C. H.; Tsai, D. P. Fundamentals and Applications of Metasurfaces. *Small Methods* **2017**, *1* (4), 1600064.
(11) Tseng, M. L.; Semmlinger, M.; Zhang, M.; Arndt, C.; Huang, T. T.; Yang, J.; Kuo, H. Y.; Su, V. C.; Chen, M. K.; Chu, C. H.; Cerjan, B.; Tsai, D. P.; Nordlander, P.; Halas, N. J. Vacuum ultraviolet nonlinear metalens. *Sci. Adv.* **2022**, *8* (16), No. eabn5644.
(12) Luo, Y.; Tseng, M. L.; Vyas, S.; Kuo, H. Y.; Chu, C. H.; Chen, M. K.; Lee, H. C.; Chen, W. P.; Su, V. C.; Shi, X.; Misawa, H.; Tsai, D. P.; Yang, P. C. Metasurface-Based Abrupt Autofocusing Beam for Biomedical Applications. *Small Methods* **2022**, *6* (4), No. e2101228.
(13) Kuznetsov, A. I.; Brongersma, M. L.; Yao, J.; Chen, M. K.; Levy, U.; Tsai, D. P.; Zheludev, N. I.; Faraon, A.; Arbabi, A.; Yu, N.; Chanda, D.; Crozier, K. B.; Kildishev, A. V.; Wang, H.; Yang, J. K. W.; Valentine, J. G.; Genevet, P.; Fan, J. A.; Miller, O. D.; Majumdar, A.; Froch, J. E.; Brady, D.; Heide, F.; Veeraraghavan, A.; Engheta, N.; Alu, A.; Polman, A.; Atwater, H. A.; Thureja, P.; Paniagua-Dominguez, R.; Ha, S. T.; Barreda, A. I.; Schuller, J. A.; Staude, I.; Grinblat, G.; Kivshar, Y.; Peana, S.; Yelin, S. F.; Senichev, A.; Shalaev, V. M.; Saha, S.; Boltasseva, A.; Rho, J.; Oh, D. K.; Kim, J.; Park, J.; Devlin, R.; Pala, R. A. Roadmap for Optical Metasurfaces. *ACS Photonics* **2024**, *11* (3), 816−865.
(14) Yu, M.-J.; Chang, C.-L.; Lan, H.-Y.; Chiao, Z.-Y.; Chen, Y.-C.; Howard Lee, H. W.; Chang, Y.-C.; Chang, S.-W.; Tanaka, T.; Tung, V.; Chou, H.-H.; Lu, Y.-J. Plasmon-Enhanced Solar-Driven Hydrogen Evolution Using Titanium Nitride Metasurface Broadband Absorbers. *ACS Photonics* **2021**, *8* (11), 3125−3132.
(15) Yuan, L.; Zhao, Y.; Toma, A.; Aglieri, V.; Gerislioglu, B.; Yuan, Y.; Lou, M.; Ogundare, A.; Alabastri, A.; Nordlander, P.; Halas, N. J. A Quasi-Bound States in the Continuum Dielectric Metasurface-Based Antenna-Reactor Photocatalyst. *Nano Lett.* **2024**, *24* (1), 172−179.
(16) Richter, F. U.; Sinev, I.; Zhou, S.; Leitis, A.; Oh, S. H.; Tseng, M. L.; Kivshar, Y.; Altug, H. Gradient High-Q Dielectric Metasurfaces for Broadband Sensing and Control of Vibrational Light-Matter Coupling. *Adv. Mater.* **2024**, *36* (25), No. e2314279.
(17) Neubrech, F.; Huck, C.; Weber, K.; Pucci, A.; Giessen, H. Surface-Enhanced Infrared Spectroscopy Using Resonant Nanoantennas. *Chem. Rev.* **2017**, *117*, 5110.
(18) Ye, L.; Li, J.; Richter, F. U.; Jahani, Y.; Lu, R.; Lee, B. R.; Tseng, M. L.; Altug, H. Dielectric Tetramer Nanoresonators Supporting Strong Superchiral Fields for Vibrational Circular Dichroism Spectroscopy. *ACS Photonics* **2023**, *10* (12), 4377−4384.
(19) Kumamoto, Y.; Taguchi, A.; Kawata, S. Deep-Ultraviolet Biomolecular Imaging and Analysis. *Adv. Opt. Mater.* **2019**, *7* (5), 1801099.
(20) Lee, B. R.; Chiang, M. F.; Ho, P. Y.; Chen, K. H.; Lee, J. H.; Hsu, P. H.; Peng, Y. C.; Hou, J. Y.; Chen, S. C.; Lee, Q. Y.; Chang, C. H.; Li, B. R.; Lin, T. E.; Lin, C. T.; Shih, M. H.; Lien, D. H.; Lin, Y. C.; Horng, R. H.; Kivshar, Y.; Tseng, M. L. Deep-UV Silicon Polaritonic Metasurfaces for Enhancing Biomolecule Autofluorescence and Two-Dimensional Material Double-Resonance Raman Scattering. *Adv. Funct. Mater.* **2025**, DOI: 10.1002/adfm.202420439.
(21) Nwokeoji, A. O.; Kilby, P. M.; Portwood, D. E.; Dickman, M. J. Accurate Quantification of Nucleic Acids Using Hypochromicity Measurements in Conjunction with UV Spectrophotometry. *Anal. Chem.* **2017**, *89* (24), 13567−13574.
(22) Ojaghi, A.; Carrazana, G.; Caruso, C.; Abbas, A.; Myers, D. R.; Lam, W. A.; Robles, F. E. Label-free hematology analysis using deep-ultraviolet microscopy. *Proc. Natl. Acad. Sci. U.S.A.* **2020**, *117* (26), 14779−14789.
(23) Kikawada, M.; Ono, A.; Inami, W.; Kawata, Y. Plasmon-Enhanced Autofluorescence Imaging of Organelles in Label-Free Cells by Deep-Ultraviolet Excitation. *Anal. Chem.* **2016**, *88* (2), 1407−1411.
(24) Gong, Y.; Gong, Z. Laser-Based Micro/Nano-Processing Techniques for Microscale LEDs and Full-Color Displays. *Adv. Mater. Technol.* **2023**, *8* (5), 2200949.
(25) Bian, J.; Zhou, L.; Wan, X.; Zhu, C.; Yang, B.; Huang, Y. Laser Transfer, Printing, and Assembly Techniques for Flexible Electronics. *Adv. Electron. Mater.* **2019**, *5* (7), 1800900.
(26) Peng, Y. C.; Wang, Y. J.; Chen, K. H.; Lin, Y. H.; Sakurai, H.; Chang, H. C.; Chiang, C. C.; Duh, R. T.; Lee, B. R.; Huang, C. Y.; et al. Deep-Ultraviolet AlN Metalens with Imaging and Ultrafast Laser Microfabrication Applications. *Nano Lett.* **2025**, *25* (8), 3141−3149.

(27) Inagaki, T.; Hamm, R. N.; Arakawa, E. T.; Painter, L. R. Optical and dielectric properties of DNA in the extreme ultraviolet. *J. Chem. Phys.* **1974**, *61* (10), 4246−4250.
(28) Liu, H. L.; Yang, T.; Tatsumi, Y.; Zhang, Y.; Dong, B.; Guo, H.; Zhang, Z.; Kumamoto, Y.; Li, M. Y.; Li, L. J.; et al. Deep-ultraviolet Raman scattering spectroscopy of monolayer WS_2. *Sci. Rep.* **2018**, *8* (1), 11398.
(29) Tanabe, I.; Tanaka, Y. Y.; Watari, K.; Inami, W.; Kawata, Y.; Ozaki, Y. Enhanced Surface Plasmon Resonance Wavelength Shifts by Molecular Electronic Absorption in Far- and Deep-Ultraviolet Regions. *Sci. Rep.* **2020**, *10* (1), 9938.
(30) Zeskind, B. J.; Jordan, C. D.; Timp, W.; Trapani, L.; Waller, G.; Horodincu, V.; Ehrlich, D. J.; Matsudaira, P. Nucleic acid and protein mass mapping by live-cell deep-ultraviolet microscopy. *Nat. Methods* **2007**, *4* (7), 567−569.
(31) Sharma, B.; Cardinal, M. F.; Ross, M. B.; Zrimsek, A. B.; Bykov, S. V.; Punihaole, D.; Asher, S. A.; Schatz, G. C.; Van Duyne, R. P. Aluminum Film-Over-Nanosphere Substrates for Deep-UV Surface-Enhanced Resonance Raman Spectroscopy. *Nano Lett.* **2016**, *16* (12), 7968−7973.
(32) Barulin, A.; Claude, J.-B.; Patra, S.; Moreau, A.; Lumeau, J.; Wenger, J. Preventing Aluminum Photocorrosion for Ultraviolet Plasmonics. *J. Phys. Chem. Lett.* **2019**, *10* (19), 5700−5707.
(33) Tittl, A.; Leitis, A.; Liu, M.; Yesilkoy, F.; Choi, D.-Y.; Neshev, D. N.; Kivshar, Y. S.; Altug, H. Imaging-based molecular barcoding with pixelated dielectric metasurfaces. *Science* **2018**, *360* (6393), 1105−1109.
(34) Jangid, P.; Richter, F. U.; Tseng, M. L.; Sinev, I.; Kruk, S.; Altug, H.; Kivshar, Y. Spectral Tuning of High-Harmonic Generation with Resonance-Gradient Metasurfaces. *Adv. Mater.* **2024**, *36* (2), No. e2307494.
(35) Yang, J. H.; Huang, Z. T.; Maksimov, D. N.; Pankin, P. S.; Timofeev, I. V.; Hong, K. B.; Li, H.; Chen, J. W.; Hsu, C. Y.; Liu, Y. Y.; et al. Low-Threshold Bound State in the Continuum Lasers in Hybrid Lattice Resonance Metasurfaces. *Laser Photonics Rev.* **2021**, *15* (10), 2100118.
(36) Malek, S. C.; Overvig, A. C.; Alu, A.; Yu, N. Multifunctional resonant wavefront-shaping meta-optics based on multilayer and multi-perturbation nonlocal metasurfaces. *Light Sci. Appl.* **2022**, *11* (1), 246.
(37) Zhang, C.; Divitt, S.; Fan, Q.; Zhu, W.; Agrawal, A.; Lu, Y.; Xu, T.; Lezec, H. J. Low-loss metasurface optics down to the deep ultraviolet region. *Light Sci. Appl.* **2020**, *9*, 55.
(38) Abdelraouf, O. A. M.; Anthur, A. P.; Wang, X. R.; Wang, Q. J.; Liu, H. Modal Phase-Matched Bound States in the Continuum for Enhancing Third Harmonic Generation of Deep Ultraviolet Emission. *ACS Nano* **2024**, *18* (5), 4388−4397.
(39) Dong, L.; Yang, X.; Zhang, C.; Cerjan, B.; Zhou, L.; Tseng, M. L.; Zhang, Y.; Alabastri, A.; Nordlander, P.; Halas, N. J. Nanogapped Au Antennas for Ultrasensitive Surface-Enhanced Infrared Absorption Spectroscopy. *Nano Lett.* **2017**, *17* (9), 5768−5774.
(40) Adato, R.; Artar, A.; Erramilli, S.; Altug, H. Engineered absorption enhancement and induced transparency in coupled molecular and plasmonic resonator systems. *Nano Lett.* **2013**, *13* (6), 2584−2591.
(41) Koshelev, K.; Lepeshov, S.; Liu, M.; Bogdanov, A.; Kivshar, Y. Asymmetric Metasurfaces with High-Q Resonances Governed by Bound States in the Continuum. *Phys. Rev. Lett.* **2018**, *121* (19), 193903.
(42) Hsu, C. W.; Zhen, B.; Stone, A. D.; Joannopoulos, J. D.; Soljačić, M. Bound states in the continuum. *Nat. Rev. Mater.* **2016**, *1*, 16048.
(43) Kühne, J.; Wang, J.; Weber, T.; Kühner, L.; Maier, S. A.; Tittl, A. Fabrication robustness in BIC metasurfaces. *Nanophotonics* **2021**, *10* (17), 4305−4312.
(44) Jackson, J. *Classical Electrodynamics*, 3rd ed.; Wiley, 1998.
(45) Ho, Y.-L.; Fong, C. F.; Wu, Y.-J.; Konishi, K.; Deng, C.-Z.; Fu, J.-H.; Kato, Y. K.; Tsukagoshi, K.; Tung, V.; Chen, C.-W. Finite-Area Membrane Metasurfaces for Enhancing Light-Matter Coupling in Monolayer Transition Metal Dichalcogenides. *ACS Nano* **2024**, *18* (35), 24173−24181.
(46) Xu, L.; Zangeneh Kamali, K.; Huang, L.; Rahmani, M.; Smirnov, A.; Camacho-Morales, R.; Ma, Y.; Zhang, G.; Woolley, M.; Neshev, D.; Miroshnichenko, A. E. Dynamic Nonlinear Image Tuning through Magnetic Dipole Quasi-BIC Ultrathin Resonators. *Adv. Sci.* **2019**, *6* (15), 1802119.
(47) Al-Ani, I. A. M.; As'Ham, K.; Huang, L.; Miroshnichenko, A. E.; Hattori, H. T. Enhanced Strong Coupling of TMDC Monolayers by Bound State in the Continuum. *Laser Photonics Rev.* **2021**, *15* (12), 2100240.
(48) Dodge, M. J. Refractive properties of magnesium fluoride. *Appl. Opt.* **1984**, *23* (12), 1980−1985.
(49) Zheng, Q.; Wang, X.; Thompson, D. Temperature-dependent optical properties of monocrystalline CaF_2, BaF_2, and MgF_2. *Opt. Mater. Express* **2023**, *13* (8), 2380−2391.
(50) Wang, Y.; Chen, Q.; Yang, W.; Ji, Z.; Jin, L.; Ma, X.; Song, Q.; Boltasseva, A.; Han, J.; Shalaev, V. M.; Xiao, S. High-efficiency broadband achromatic metalens for near-IR biological imaging window. *Nat. Commun.* **2021**, *12* (1), 5560.
(51) Wang, S.; Wu, P. C.; Su, V. C.; Lai, Y. C.; Chen, M. K.; Kuo, H. Y.; Chen, B. H.; Chen, Y. H.; Huang, T. T.; Wang, J. H.; Lin, R. M.; Kuan, C. H.; Li, T.; Wang, Z.; Zhu, S.; Tsai, D. P. A broadband achromatic metalens in the visible. *Nat. Nanotechnol.* **2018**, *13* (3), 227−232.
(52) Nojiri, K. Latest Dry Etching Technologies. In *Dry Etching Technology for Semiconductors*, Nojiri, K., Ed.; Springer International Publishing, 2015; pp 91−112.
(53) Son, H. J.; Efremov, A.; Choi, G.; Kwon, K.-H. Individual Effects of Various Plasma-Related Factors on the High Aspect Ratio Oxide Etching Process at Low-Frequency Bias Power Using an Inductively Coupled Plasma System. *Plasma Chem. Plasma Process.* **2024**, *44* (1), 635−649.
(54) Johnson, E. G.; Donohue, L. A.; Nordin, G. P.; Hopkins, J.; Barnett, R.; Newton, A.; Barker, A. Developments in Si and SiO_2 etching for MEMS-based optical applications. *Micromachining Technology for Micro-Optics and Nano-Optics II* **2003**, *5347*, na.
(55) Fukasawa, T.; Nakamura, A.; Shindo, H.; Yasuhiro Horiike, Y. H. High Rate and Highly Selective SiO2 Etching Employing Inductively Coupled Plasma. *Jpn. J. Appl. Phys.* **1994**, *33* (4S), 2139.
(56) Li, H.; Xie, C. Fabrication of Ultra-High Aspect Ratio (>420:1) Al_2O_3 Nanotube Arraysby Sidewall TransferMetal Assistant Chemical Etching. *Micromachines* **2020**, *11* (4), 378.
(57) Jha, S. K.; Ahmed, Z.; Agio, M.; Ekinci, Y.; Löffler, J. F. Deep-UV Surface-Enhanced Resonance Raman Scattering of Adenine on Aluminum Nanoparticle Arrays. *J. Am. Chem. Soc.* **2012**, *134* (4), 1966−1969.
(58) Barulin, A.; Claude, J. B.; Patra, S.; Bonod, N.; Wenger, J. Deep Ultraviolet Plasmonic Enhancement of Single Protein Autofluorescence in Zero-Mode Waveguides. *Nano Lett.* **2019**, *19* (10), 7434−7442.
(59) Kavungal, D.; Magalhaes, P.; Kumar, S. T.; Kolla, R.; Lashuel, H. A.; Altug, H. Artificial intelligence-coupled plasmonic infrared sensor for detection of structural protein biomarkers in neurodegenerative diseases. *Sci. Adv.* **2023**, *9* (28), No. eadg9644.
(60) Xu, K.; Zhou, R.; Takei, K.; Hong, M. Toward Flexible Surface-Enhanced Raman Scattering (SERS) Sensors for Point-of-Care Diagnostics. *Adv. Sci.* **2019**, *6* (16), 1900925.
(61) Tittl, A.; John-Herpin, A.; Leitis, A.; Arvelo, E. R.; Altug, H. Metasurface-Based Molecular Biosensing Aided by Artificial Intelligence. *Angew. Chem., Int. Ed. Engl.* **2019**, *58* (42), 14810−14822.
(62) Ulman, A. Formation and Structure of Self-Assembled Monolayers. *Chem. Rev.* **1996**, *96* (4), 1533−1554.
(63) Adato, R.; Yanik, A. A.; Amsden, J. J.; Kaplan, D. L.; Omenetto, F. G.; Hong, M. K.; Erramilli, S.; Altug, H. Ultra-sensitive vibrational spectroscopy of protein monolayers with plasmonic nanoantenna arrays. *Proc. Natl. Acad. Sci. U. S. A.* **2009**, *106* (46), 19227−19232.
(64) Fahrenkopf, N. M.; Rice, P. Z.; Bergkvist, M.; Deskins, N. A.; Cady, N. C. Immobilization mechanisms of deoxyribonucleic acid

(DNA) to hafnium dioxide (HfO_2) surfaces for biosensing applications. *ACS Appl. Mater.* **2012**, *4* (10), 5360−5368.
(65) Midwood, K. S.; Carolus, M. D.; Danahy, M. P.; Schwarzbauer, J. E.; Schwartz, J. Easy and efficient bonding of biomolecules to an oxide surface of silicon. *Langmuir* **2004**, *20* (13), 5501−5505.
(66) Wang, I. S.; Lin, Y. T.; Huang, C. H.; Lu, T. F.; Lue, C. E.; Yang, P.; Pijanswska, D. G.; Yang, C. M.; Wang, J. C.; Yu, J. S.; Chang, Y. S.; Chou, C.; Lai, C. S. Immobilization of enzyme and antibody on ALD-HfO_2-EIS structure by NH_3 plasma treatment. *Nanoscale Res. Lett.* **2012**, *7* (1), 179.
(67) Lee, M.; Zine, N.; Baraket, A.; Zabala, M.; Campabadal, F.; Caruso, R.; Trivella, M. G.; Jaffrezic-Renault, N.; Errachid, A. A novel biosensor based on hafnium oxide: Application for early stage detection of human interleukin-10. *Sens. Actuators B: Chem.* **2012**, *175*, 201−207.
(68) Cerjan, B.; Halas, N. J. Toward a Nanophotonic Nose: A Compressive Sensing-Enhanced, Optoelectronic Mid-Infrared Spectrometer. *ACS Photonics* **2019**, *6* (1), 79−86.
(69) Ho, C. S.; Jean, N.; Hogan, C. A.; Blackmon, L.; Jeffrey, S. S.; Holodniy, M.; Banaei, N.; Saleh, A. A. E.; Ermon, S.; Dionne, J. Rapid identification of pathogenic bacteria using Raman spectroscopy and deep learning. *Nat. Commun.* **2019**, *10* (1), 4927.
(70) Leitis, A.; Tseng, M. L.; John-Herpin, A.; Kivshar, Y. S.; Altug, H. Wafer-Scale Functional Metasurfaces for Mid-Infrared Photonics and Biosensing. *Adv. Mater.* **2021**, *33* (43), No. e2102232.
(71) Xiang, Y.; Wu, S.; Du, A.; Zhang, Z.; Shen, J.; Zhou, B. A new approach for preparation of free-standing nano-porous SiO_2 films with a large area. *J. Sol-Gel Sci. Technol.* **2016**, *80* (2), 267−276.
(72) Novikov, S.; Sinkkonen, J.; Nikitin, T.; Khriachtchev, L.; Räsänen, M.; Haimi, E. Free-standing SiO_2 films containing Si nanocrystals directly suitable for transmission electron microscopy. *Microelectronics Journal* **2008**, *39* (3), 518−522.
(73) Han, S.; Meng, Y.; Xu, Z.; Kim, J. S.; Li, Y.; Roh, I.-P.; Ahn, H.; Kim, D.-H.; Bae, S.-H. Freestanding Membranes for Unique Functionality in Electronics. *ACS Appl. Electron. Mater.* **2023**, *5* (2), 690−704.
(74) Storm, A. J.; Storm, C.; Chen, J.; Zandbergen, H.; Joanny, J. F.; Dekker, C. Fast DNA translocation through a solid-state nanopore. *Nano Lett.* **2005**, *5* (7), 1193−1197.
(75) Storm, A. J.; Chen, J. H.; Ling, X. S.; Zandbergen, H. W.; Dekker, C. Fabrication of solid-state nanopores with single-nanometre precision. *Nat. Mater.* **2003**, *2* (8), 537−540.
(76) Lu, Y. H.; Morales, C.; Zhao, X.; van Spronsen, M. A.; Baskin, A.; Prendergast, D.; Yang, P.; Bechtel, H. A.; Barnard, E. S.; Ogletree, D. F.; Altoe, V.; Soriano, L.; Schwartzberg, A. M.; Salmeron, M. Ultrathin Free-Standing Oxide Membranes for Electron and Photon Spectroscopy Studies of Solid-Gas and Solid-Liquid Interfaces. *Nano Lett.* **2020**, *20* (9), 6364−6371.
(77) Liu, T.; Ou, J.-Y.; MacDonald, K. F.; Zheludev, N. I. Photonic metamaterial analogue of a continuous time crystal. *Nat. Phys.* **2023**, *19* (7), 986−991.
(78) Fang, X.; Tseng, M. L.; Tsai, D. P.; Zheludev, N. I. Coherent Excitation-Selective Spectroscopy of Multipole Resonances. *Phys. Rev. Appl.* **2016**, *5* (1), 014010.
(79) Konishi, K.; Akai, D.; Mita, Y.; Ishida, M.; Yumoto, J.; Kuwata-Gonokami, M. Circularly polarized vacuum ultraviolet coherent light generation using a square lattice photonic crystal nanomembrane. *Optica* **2020**, *7* (8), 855−863.
(80) Zhang, X.; Cai, H.; Rezaei, S. D.; Rosenmann, D.; Lopez, D. A universal metasurface transfer technique for heterogeneous integration. *Nanophotonics* **2023**, *12* (8), 1633−1642.
(81) Chu, C. H.; Tseng, M. L.; Chen, J.; Wu, P. C.; Chen, Y.-H.; Wang, H.-C.; Chen, T.-Y.; Hsieh, W. T.; Wu, H. J.; Sun, G.; Tsai, D. P. Active dielectric metasurface based on phase-change medium. *Laser Photonics Rev.* **2016**, *10* (6), 1063−1063.
(82) Arbabi, E.; Arbabi, A.; Kamali, S. M.; Horie, Y.; Faraji-Dana, M.; Faraon, A. MEMS-tunable dielectric metasurface lens. *Nat. Commun.* **2018**, *9* (1), 812.
(83) Hentschel, M.; Schaferling, M.; Duan, X.; Giessen, H.; Liu, N. Chiral plasmonics. *Sci. Adv.* **2017**, *3* (5), No. e1602735.
(84) Ji, R.; Wang, S.-W.; Liu, X.; Guo, H.; Lu, W. Hybrid Helix Metamaterials for Giant and Ultrawide Circular Dichroism. *ACS Photonics* **2016**, *3* (12), 2368−2374.
(85) Tseng, M. L.; Lin, Z. H.; Kuo, H. Y.; Huang, T. T.; Huang, Y. T.; Chung, T. L.; Chu, C. H.; Huang, J. S.; Tsai, D. P. Stress-Induced 3D Chiral Fractal Metasurface for Enhanced and Stabilized Broadband Near-Field Optical Chirality. *Adv. Opt. Mater.* **2019**, *7* (15), 1900617.
(86) Duan, X.; Kamin, S.; Sterl, F.; Giessen, H.; Liu, N. Hydrogen-Regulated Chiral Nanoplasmonics. *Nano Lett.* **2016**, *16* (2), 1462−1466.
(87) Shi, T.; Deng, Z. L.; Geng, G.; Zeng, X.; Zeng, Y.; Hu, G.; Overvig, A.; Li, J.; Qiu, C. W.; Alu, A.; Kivshar, Y. S.; Li, X. Planar chiral metasurfaces with maximal and tunable chiroptical response driven by bound states in the continuum. *Nat. Commun.* **2022**, *13* (1), 4111.
(88) Gorkunov, M. V.; Antonov, A. A.; Kivshar, Y. S. Metasurfaces with Maximum Chirality Empowered by Bound States in the Continuum. *Phys. Rev. Lett.* **2020**, *125* (9), 093903.
(89) Overvig, A. C.; Malek, S. C.; Yu, N. Multifunctional Nonlocal Metasurfaces. *Phys. Rev. Lett.* **2020**, *125* (1), 017402.
(90) Ki, Y. G.; Jeon, B. J.; Song, I. H.; Kim, S. J.; Jeon, S.; Kim, S. J. Realizing Minimally Perturbed, Nonlocal Chiral Metasurfaces for Direct Stokes Parameter Detection. *ACS Nano* **2024**, *18* (9), 7064−7073.
(91) Kenney, M.; Li, S.; Zhang, X.; Su, X.; Kim, T. T.; Wang, D.; Wu, D.; Ouyang, C.; Han, J.; Zhang, W.; Sun, H.; Zhang, S. Pancharatnam-Berry Phase Induced Spin-Selective Transmission in Herringbone Dielectric Metamaterials. *Adv. Mater.* **2016**, *28* (43), 9567−9572.
(92) Plum, E.; Fedotov, V. A.; Zheludev, N. I. Extrinsic electromagnetic chirality in metamaterials. *J. Opt. A: Pure Appl. Opt.* **2009**, *11* (7), 074009.
(93) Fedotov, V. A.; Mladyonov, P. L.; Prosvirnin, S. L.; Rogacheva, A. V.; Chen, Y.; Zheludev, N. I. Asymmetric propagation of electromagnetic waves through a planar chiral structure. *Phys. Rev. Lett.* **2006**, *97* (16), 167401.

https://doi.org/10.1021/acsphotonics.4c01960
ACS Photonics 2025, 12, 2955−2964